

Electronic Supplementary Information

Gating and tunable confinement of active colloids within patterned environments

Carolina van Baalen^{*a}, Stefania Ketzetzi^{*ab}, Anushka Tintor^a, Israel Gabay^c, Lucio Isa^a

^aLaboratory for Soft Materials and Interfaces, Department of Materials, ETH Zürich, Vladimir-Prelog-Weg 5, 8093 Zürich, Switzerland

^b Present address: John A. Paulson School of Engineering and Applied Sciences, Harvard University, Cambridge, MA 02138, USA

^c Faculty of Mechanical Engineering, Technion – Israel Institute of Technology, Haifa 3200003, Israel

* These authors contributed equally to this work.

Corresponding author: lucio.isa@mat.ethz.ch

S1. Microswimmer self-propulsion speeds under an electric field

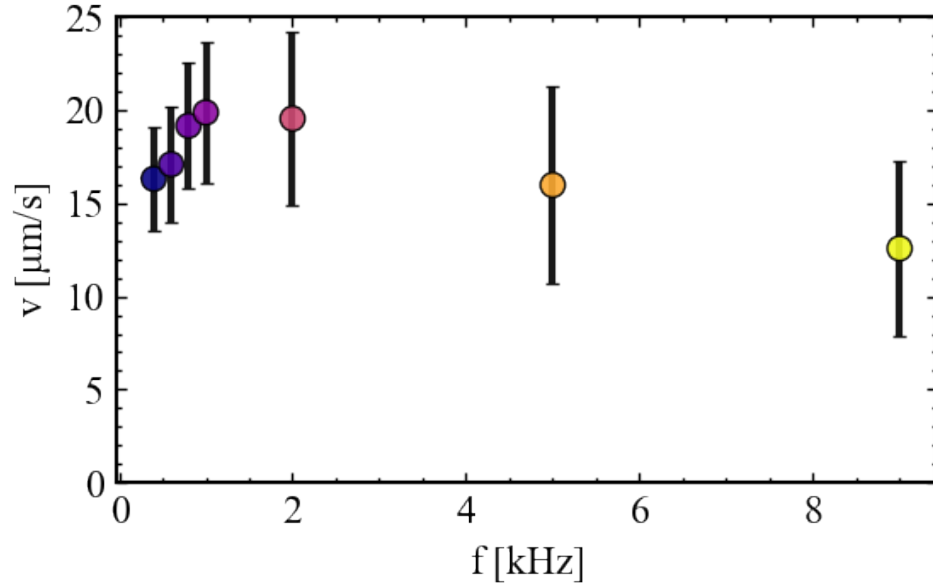


Figure S1: **Microswimmer self-propulsion speed under an electric field.** Active velocities of metallodielectric Janus spheres composed of a $3 \mu\text{m}$ SiO_2 core and a 6.5 nm Pd cap as a function of the frequency of the applied alternating current (AC) electric field. Data was obtained at a fixed peak-to-peak voltage of $V_{pp} = 6 \text{ V}$. Self-propulsion speeds were extracted from a least-squares fit of the individual mean squared displacements of approximately 60 microswimmers.

S2. Microswimmer self-propulsion speeds upon approaching a cylindrical obstacle

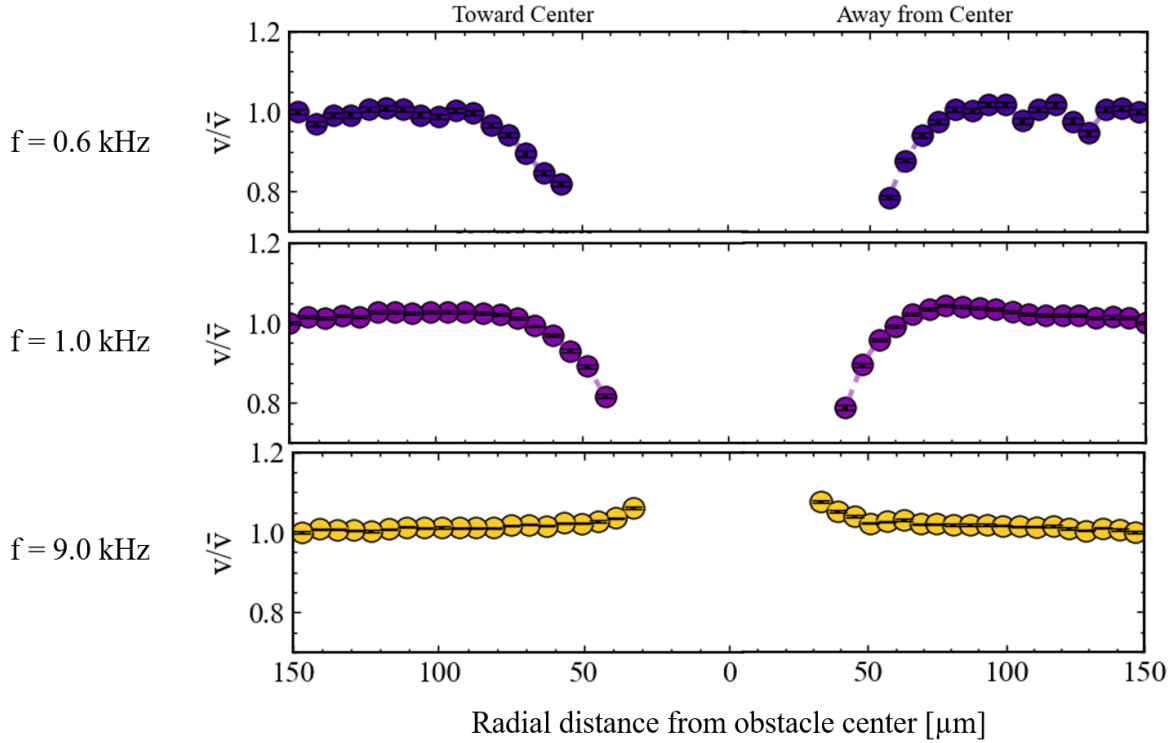


Figure S2: **Mean normalized self-propulsion velocity *versus* radial distance from an obstacle.** Mean normalized magnitude of the velocity of the same Pd-capped Janus microswimmers as in Fig. S1 and the main text, as a function of radial distance from a cylindrical obstacle with a height of $6 \mu\text{m}$ and a diameter of $10 \mu\text{m}$, at a fixed peak-to-peak voltage of $V_{pp} = 6 \text{ V}$ and varying frequencies. The center of the pillar is indicated by $x = 0$. Self-propulsion speeds were calculated from the magnitude of the displacement vector over a 100 msec time interval.

S3. Time-averaged density maps in the active state (Janus spheres)

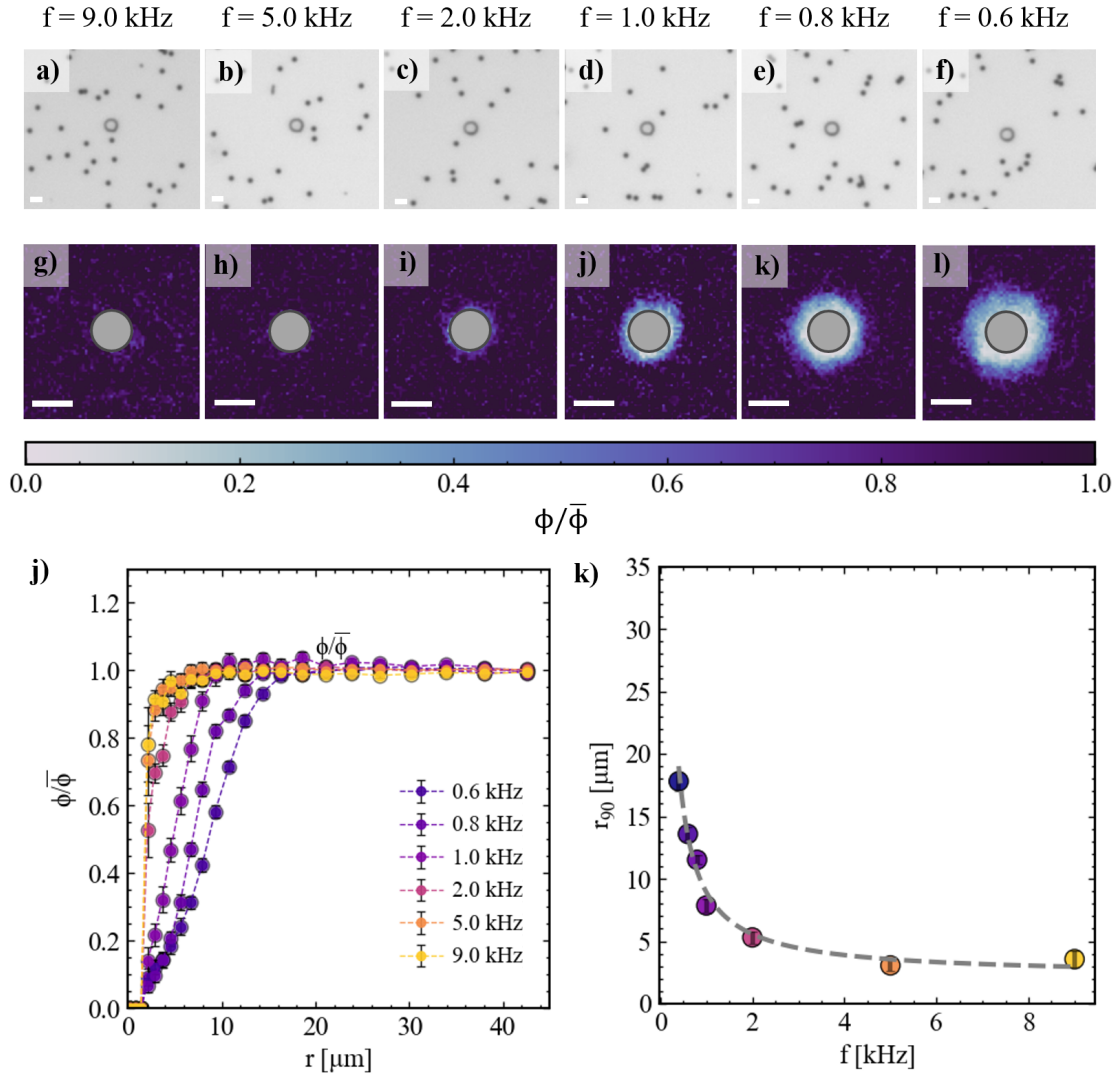


Figure S3: **Detailed data of microswimmer obstacle avoidance via electric field frequency modulation (active state).** a-f) Bright-field microscopy images of a sample depicting Janus Pd-capped active colloids ($R=2.96 \mu\text{m}$ SiO_2 spheres with 6.5 nm Pd coating) in proximity to a cylindrical obstacle with height $6 \mu\text{m}$ and diameter $10 \mu\text{m}$ under a fixed 6 V peak-to-peak amplitude and varying frequency from $f = 9.0 - 0.6$ kHz. g-l) Time-averaged Janus microswimmer density profiles corresponding to a-f, normalized by the time-averaged density in the sample far away from the obstacle. j) Normalized microswimmer density as a function of radial distance from the obstacle surface for frequencies ranging from $f = 9.0 - 0.6$ kHz. k) Microswimmer-obstacle separation distance at a time-averaged microswimmer density corresponding to 0.9 times the density far away from the obstacle, i.e. r_{90} , as a function of the frequency. Scale bars are $10 \mu\text{m}$.

S4. Dynamics of metallo-dielectric Janus microswimmers of varying size and composition interacting with obstacles

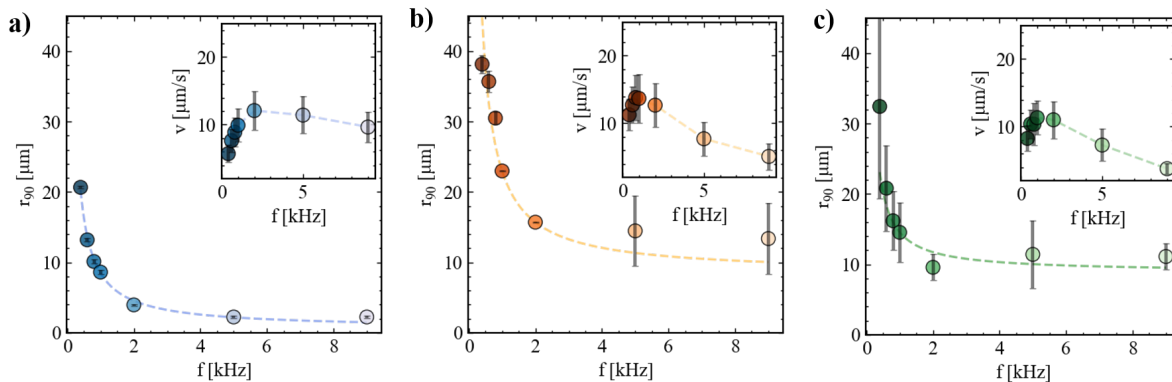


Figure S4: **Dynamics of metallo-dielectric Janus microswimmers of varying size and composition.** Microswimmer-obstacle separation distance at a time-averaged microswimmer density corresponding to 0.9 times the density far away from the obstacle (denoted as r_{90}), as a function of frequency, for the various metallo-dielectric Janus particles: a) SiO₂ core particles with a radius of $2R = 2\mu\text{m}$ and a 6.5 nm Pd cap, b) polystyrene (PS) core particles of $2R = 3\mu\text{m}$ and a 6.5 nm Pd cap, and c) SiO₂ core particles of $2R = 3\mu\text{m}$ and a 8.0 nm Au cap. Dashed lines represent a $r_{90} \propto \frac{1}{f}$ fit. Insets show the corresponding self-propulsion velocities of the different microswimmers as a function of frequency. Data were obtained at a fixed peak-to-peak voltage of $V_{pp} = 6$ V. Self-propulsion speeds were extracted from a least-squares fit to the individual mean squared displacements of approximately 60 microswimmers.

S5. Visualization of flow fields around the obstacles using tracer particles

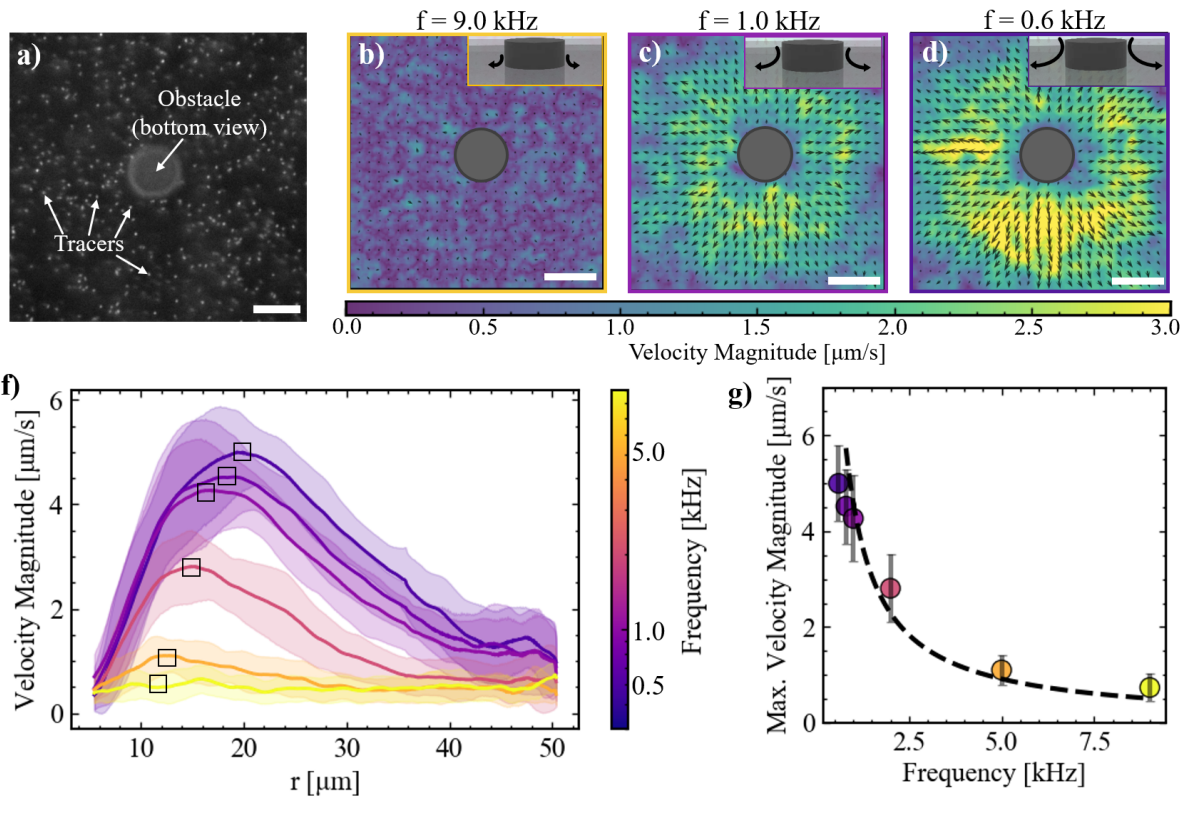


Figure S5: **Visualization of flow fields around the obstacles using tracer particles.** a) Fluorescence microscopy image showing 200 nm polystyrene tracers around a cylindrical obstacle (diameter 10 μm , height 6 μm), taken at the focal plane where the pillar is attached to the bottom electrode. The velocity direction (black arrows) and magnitude (color scale) in the 2D plane were extracted using image velocimetry from 10-second video recordings at 10 fps, under a fixed $V_{pp} = 6$ V peak-to-peak amplitude and frequencies of b) 9.0 kHz, c) 1.0 kHz, and d) 0.6 kHz. As the frequency decreases, the magnitude of the flow field increases, as schematically shown in the insets. f) Mean velocity magnitude outward from the cylindrical obstacle as a function of radial distance from the pillar at frequencies ranging from 0.6 to 9.0 kHz. g) Maximum mean velocity magnitude (black squares in f) as a function of frequency. The dashed line indicates a $v_{\text{max}} \propto \frac{1}{f}$ fit. Scale bars are 10 μm .

S6. Time-averaged density maps in the passive state (bare spheres)

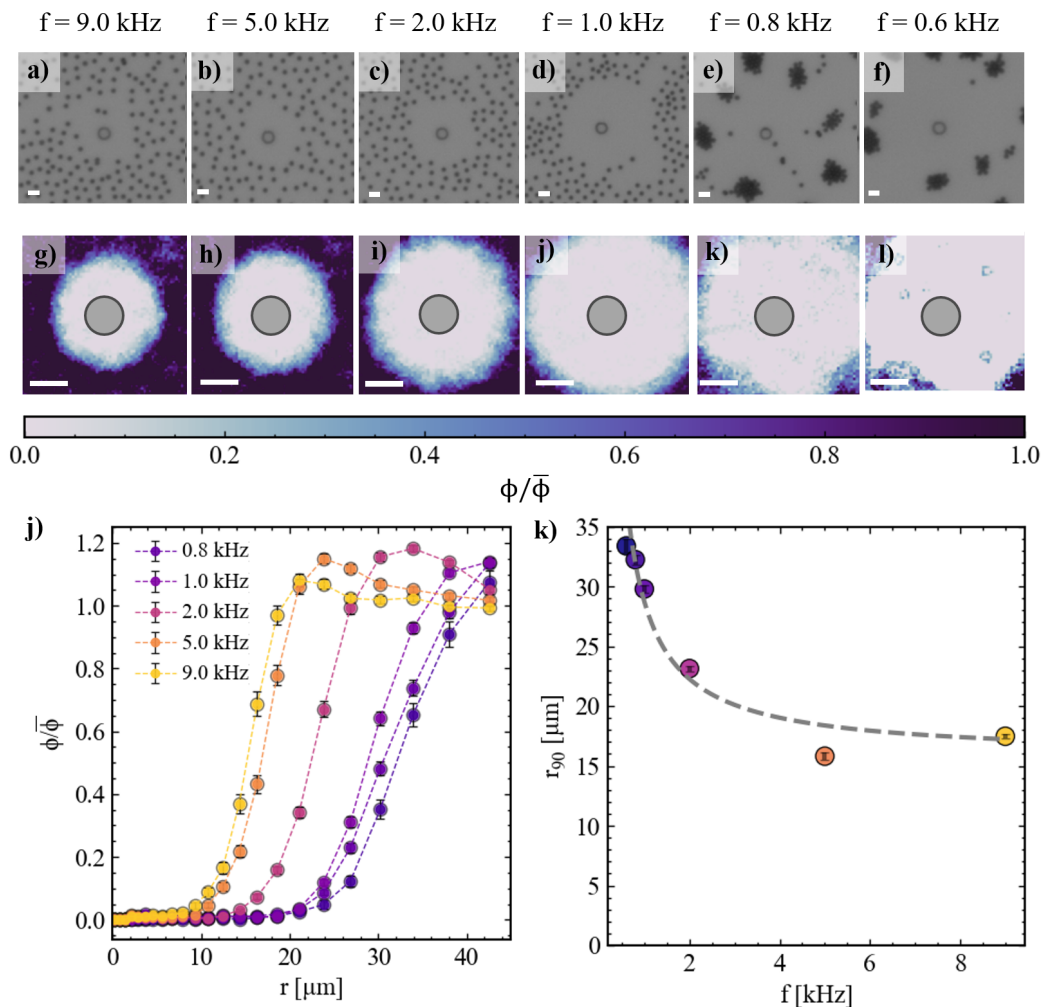


Figure S6: **Detailed data of bare SiO₂ colloids as a function of the electric field frequency (passive state).** a-f) Bright-field microscopy images of a sample depicting how bare SiO₂ colloids (bare version of metallo-dielectric Janus particles in Fig. S3) distribute and self-organize in proximity to a cylindrical obstacle with height 6 μm and radius 10 μm under a fixed 6 V peak-to-peak amplitude and varying frequency. At frequencies between 9.0-1.0 kHz, the colloids remain far from the obstacle and each other, while at frequencies below 1.0 kHz they form aggregates, differently from the corresponding Pd-capped particles in the active state in Fig. S3. g-l) Time-averaged particle density profiles corresponding to a-f, normalized by the time-averaged density in the sample far away from the obstacle. j) Normalized particle density as a function of radial distance from the obstacle surface for the same frequencies. k) Particle-obstacle separation distance at a time-averaged particle density corresponding to 0.9 times the density far from the obstacle, i.e. r_{90} , with frequency. Scale bars are 10 μm.

S7. Quantification of the role of dielectrophoretic forces

To quantify the role of dielectrophoretic (DEP) forces, we performed numerical simulations using COMSOL Multiphysics 5.3a to compute the electric potential distribution and, subsequently, the electric field gradients in the absence of particles. The simulated geometry consisted of a 3D unit cell with a width and depth of 240 μm and a height (distance between electrodes) of 120 μm . A single dielectric pillar was placed at the center of the bottom electrode, with a height of 6 μm and a diameter of 10 μm , as in the experiments. An alternating current (AC) electric potential was applied to the upper electrode, while the lower electrode was grounded. To account for frequency-dependent effects, we used a complex permittivity formulation:

$$\tilde{\epsilon} = \epsilon_0 \epsilon_r - \frac{i\sigma}{\omega} \quad (1)$$

where ϵ_0 is the vacuum permittivity, ϵ_r is the relative permittivity, σ is the electric conductivity, and ω is the frequency of the applied electric potential.

From the numerical solution, we computed the gradient of the squared electric field magnitude $\Delta|E^2|$, which determines the direction and magnitude of the DEP force. For all relevant frequencies, we found that the electric field gradient is directed toward the pillar in regions below the pillar height.

As expected, a particle more polarizable than the surrounding medium experiences positive DEP, meaning it moves in the direction of the electric field gradient $\nabla|E^2|$ and is attracted toward the pillar. Conversely, a less polarizable particle experiences negative DEP and is repelled by the pillar. To calculate the actual DEP force on a homogeneous particle, we used the COMSOL-generated field data and the classical time-averaged DEP force expression:

$$\mathbf{F}_{\text{DEP}} = 2\pi\epsilon_m R^3 \text{Re} \left[\frac{\tilde{\epsilon}_p - \tilde{\epsilon}_m}{\tilde{\epsilon}_p + 2\tilde{\epsilon}_m} \right] \nabla |\mathbf{E}_{\text{rms}}^2| \quad (2)$$

where R is the particle radius, $\tilde{\epsilon}_p$ and $\tilde{\epsilon}_m$ are the complex permittivities of the particle and the medium, respectively. The Clausius-Mossotti factor was computed using the MyDEP software¹, which also provided numerical estimates of the DEP force for both gold and silica particles across the relevant frequency range.

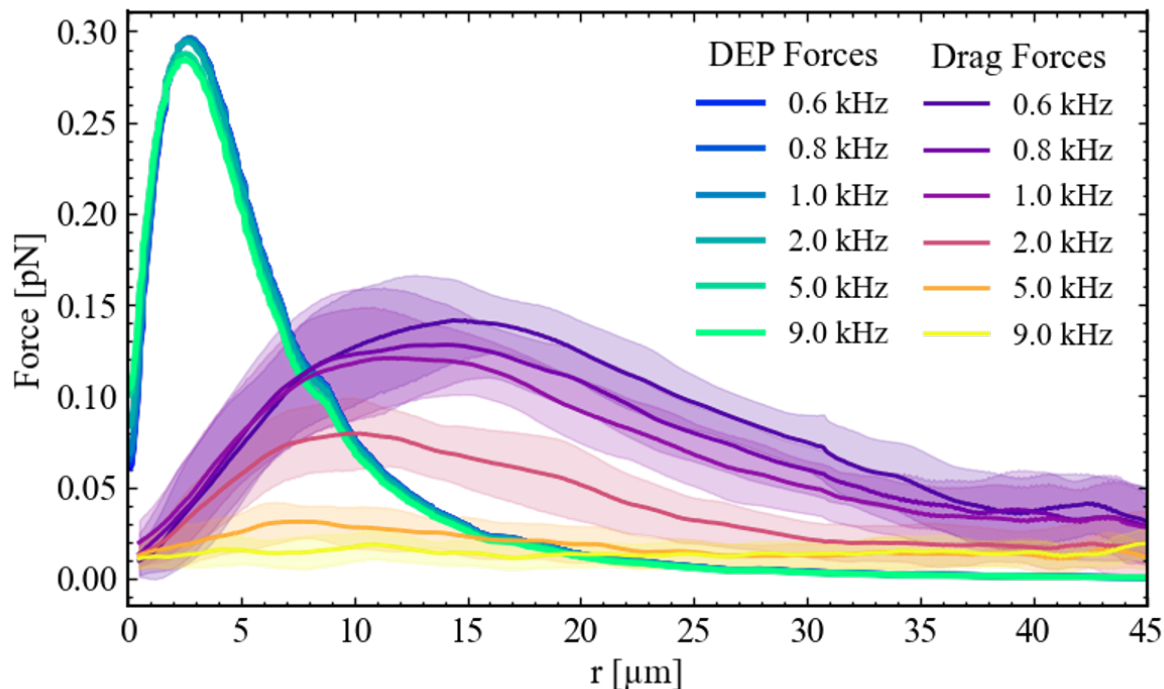


Figure S7: **Comparison of DEP forces and drag force acting on microswimmers.** The DEP forces acting on a silica sphere with a radius of $1.5 \mu\text{m}$, calculated as described above, are compared with the drag forces estimated from the fluid velocity shown in Fig. S5 using the Stokes' drag for a particle with a radius of $1.5 \mu\text{m}$. Forces are plotted as a function of radial distance from the obstacle (pillar) surface. The comparison is made under varying frequency and a fixed peak-to-peak voltage of $V_{pp} = 6 \text{ V}$. The DEP forces are of shorter range than the drag forces acting on a SiO_2 sphere, highlighting the difference in their spatial behavior across frequencies.

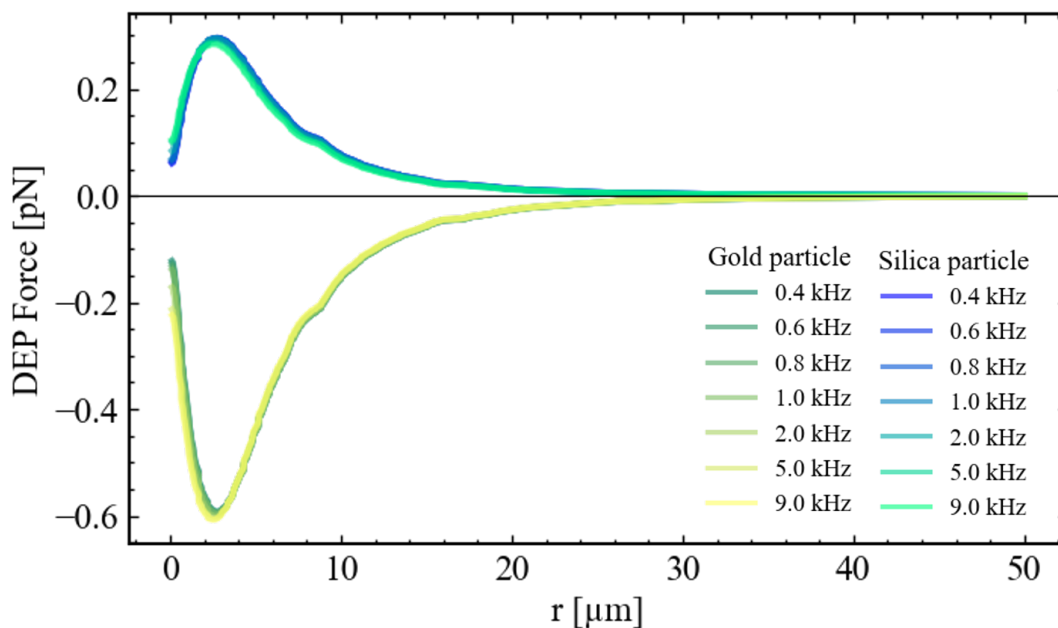


Figure S8: **Comparison of DEP forces acting on a silica versus gold particle.** The DEP forces, calculated as described above, are shown as a function of radial distance from the pillar surface, acting on a $1.5 \mu\text{m}$ radius gold or silica particle. The calculations were performed at varying frequencies and a fixed peak-to-peak voltage of 6 V. The DEP force acting on the gold particle is attractive, while the DEP force acting on the silica particle is repulsive, demonstrating the distinct polarization behaviors of the two materials, which might contribute to the turn-away response of the metallo-dielectric Janus microswimmers upon approaching an obstacle.

S8. Dependence of the exclusion zone on field strength

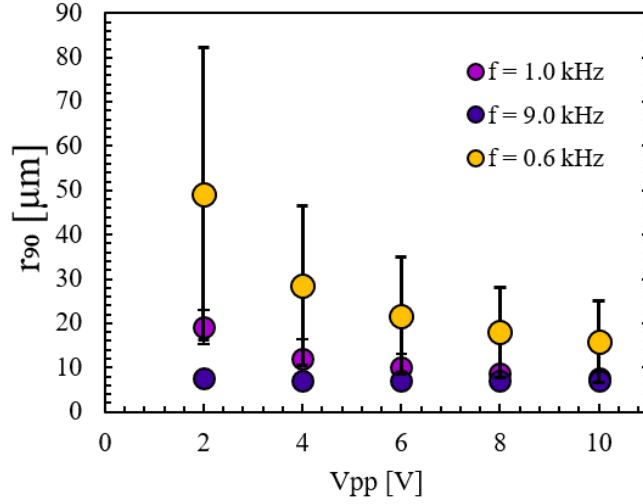


Figure S9: **Dependence of the exclusion zone on field strength.** The separation distance between microswimmers and obstacles, measured at a time-averaged microswimmer density corresponding to 0.9 times the density at infinite distance from the obstacle (denoted as r_{90}), as a function of the applied peak-to-peak voltage at fixed frequencies of 0.6, 1.0, and 9.0 kHz. Microswimmers are Pd-capped SiO_2 spheres, and the cylindrical obstacles have a height of 6 μm and a diameter of 10 μm .

S9. List of Supplementary Videos

- **Video S1:** A video showcasing the dynamics of a metallo-dielectric Janus particle, subjected to an alternating current (AC) electric field, as it approaches a cylindrical obstacle printed on the bottom electrode. The particle motion is observed under varying frequencies of the applied electric field, with a fixed peak-to-peak voltage of $V_{pp} = 6$ V. The particle trajectories are color-coded according to displacement speed, with lighter blue indicating faster speeds. This video corresponds to the snapshots in Figure 1b-d of the main text. The video has been sped up by a factor of 5.
- **Video S2:** A video showing the active trajectories of colloids self-propelling through an obstacle array, where the lattice spacing is $10\ \mu\text{m}$ in the x-direction and $35\ \mu\text{m}$ in the y-direction. The array is designed to form a path with a 90° bend. The particle dynamics are observed under varying frequencies of the applied electric field, with a fixed peak-to-peak voltage of $V_{pp} = 6$ V. This video corresponds to the snapshots in Figure 3d-f of the main text. The video has been sped up by a factor of 5.
- **Video S3:** Video showing the tunable confinement of synthetic microswimmers within a disordered environment. The active colloid trajectories are observed as they navigate through a disordered array of cylindrical obstacles. The particle dynamics are observed under varying frequencies of the applied electric field, with a fixed peak-to-peak voltage of $V_{pp} = 6$ V. This video corresponds to the snapshots in Figure 4a-c of the main text. The video has been sped up by a factor of 5.
- **Video S4:** Florescent microscopy images of fluorescent polystyrene (PS) tracer particles with a diameter of $2R = 200\ \text{nm}$ suspended in a medium surrounding a 3D-printed dielectric pillar of height $6\ \mu\text{m}$ and diameter $10\ \mu\text{m}$. The system was subjected to an applied AC electric field with a peak-to-peak voltage of $V_{pp} = 6$ V and varying frequencies. The video has been sped up by a factor of 2.

References

- [1] J. Cottet and et al., *Biophysical Journal*, 2019, **116**, 12–18.